Parametric Characterization of SGP4 Theory and TLE Positional Accuracy

Daniel L. Oltrogge
Sr. Research Astrodynamicist, Center for Space Stds. and Innovation, Analytical Graphics Inc.
Jens Ramrath
Systems Engineer, Product Support, Analytical Graphics Inc.

1. ABSTRACT

To gain better insight into the practical limits of applicability for TLEs, SGP4 and the underlying GP theory, the native SGP4 accuracy is parametrically examined for the statistically-significant range of RSO orbit inclinations experienced as a function of all orbit altitudes from LEO through GEO disposal altitude. For each orbit altitude, reference or "truth" orbits were generated using full force modeling, time-varying space weather, and AGI's HPOP numerical integration orbit propagator. Then, TLEs were optimally fit to these truth orbits. The resulting TLEs were then propagated and positionally differenced with the truth orbits to determine how well the GP theory was able to fit the truth orbits. Resultant statistics characterizing these empirically-derived accuracies are provided.

2. INTRODUCTION

Two-Line Elements, or TLEs, contain mean element state vectors compatible with General Perturbations (GP) singly-averaged semi-analytic orbit theory. This theory, embodied in the SGP4 orbit propagator, provides sufficient accuracy for some (but perhaps not all) orbit operations and SSA tasks. For more demanding tasks, higher accuracy orbit and force model approaches (i.e. "Special Perturbations" numerical integration or SP) may be required.

In recent times, the suitability of TLEs or GP theory for any SSA analysis has been increasingly questioned. Meanwhile, SP is touted as being of high quality and well-suited for most, if not all, SSA applications. Yet the lack of independent and unbiased "truth" or well-known reference orbits that haven't already been adopted for radar and optical sensor network calibration has typically prevented a truly unbiased assessment of such assertions.

This study empirically and parametrically demonstrates the ability of "Enhanced GP" (EGP) to fit notional "truth orbits" derived from using a full-force modeling, and how the EGP TLEs' resultant orbit position degrades from "truth" as a function of subsequent propagation time. To gain better insight into the practical limits of applicability for TLEs, SGP4 and the underlying GP theory, we will examine the native accuracy of the SGP4 orbit propagator and its underlying theory parametrically for the statistically-significant range of RSO orbit inclinations experienced as a function of all orbit altitudes from LEO through GEO disposal altitude. For each orbit altitude, reference or "truth" orbits are generated using full force modeling, time-varying space weather, and AGI's HPOP numerical integration orbit propagator. Then, TLEs are optimally fit to these truth orbits. The resulting TLEs were then propagated and positionally differenced with the truth orbits to determine how well the GP theory is able to fit the truth orbits. And finally, the resultant statistics characterizing these empirically-derived accuracies are provided.

Comparison plots span the entire altitude regime from 350 km to GEO for multiple orbit orientations (inclination, RAAN). Note that this approach only assesses the ability of EGP to fit a "truth orbit," and that additional errors (potentially large) could be introduced in the operational EGP implementation if the underlying SP ephemerides have errors.

3. ENHANCED GP TLE PROCESS

Multiple strategies have been devised for creating "enhanced TLEs" to reduce the errors inherent in TLE Orbit Determination (OD). These strategies seem to fall into one of two categories:

- Type 1: Perform OD using a numerical and/or Higher-Order Theory (HOT) to create "pseudo-observations and fit TLEs to those pseudo-observations [1, 2]
- Type 2: Use time histories of the TLE elements themselves or derived TLE products (e.g. simulated look angle observations, etc) to perform a second-stage TLE OD process[3, 4, 5, 6, 7]

The Type 1 TLE fit process adopted for this paper's parametrically-generated "truth orbits" was intentionally designed to mimic the JSpOC process operationally used to generate EGP TLEs for debris objects. This allows us to infer additional conclusions of the expected accuracies of EGP TLEs as currently produced by JSpOC. After a

decade of prototyping, testing and policy decisions, JSpOC now generates TLEs for orbital debris. As depicted in **Fig. 1**, this process is accomplished by **(1)** performing OD of SSN observations over a "higher-order theory" (HOT, e.g. Special Perturbations or SP numerical integration) fit span of ≈ five days; **(2)** propagate the HOT-derived numerical solution to populate "pseudo-observations" throughout an extrapolation fit span; **(3)** fit Enhanced General Perturbations (EGP) TLEs to the extrapolated SP pseudo-observations.

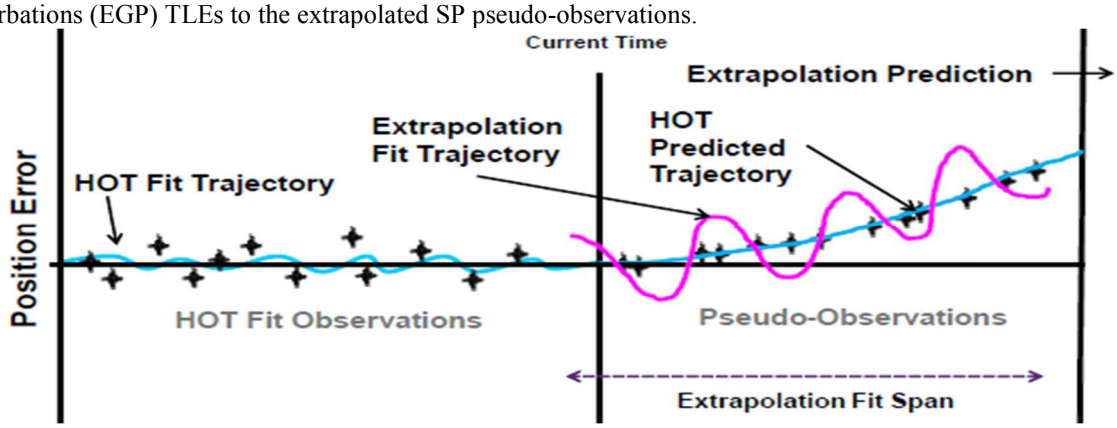

Fig. 1: Depiction of Enhanced General Perturbations (EGP) TLE fit process

4. RESEARCH MOTIVATION FOR THIS PAPER

TLEs are commonly used for SSA by the space operations community for a wide variety of applications:

(1) When initializing more detailed tracking, commanding processes which have limited initialization accuracy requirements;
(2) During the launch process, when the large uncertainties of launch (winds aloft, guidance, performance) can cause difficulties acquiring new spacecraft;
(3) During anomalies, when the primary operational process for OD may be offline or errant;
(4) When no higher-accuracy data is available for SSA;
(5) For top-level characterization of the current space active and debris populations.

TLEs are often the only available data source for a large segment of the commercial and global operator community. So for all of the above uses, it is vital that these computationally-efficient, globally available TLE orbit states be as accurate as possible.

Yet TLEs have been criticized by some as being of insufficient accuracy for SSA work, often accompanied by unsubstantiated statements that SP-quality data is the only data of sufficient accuracy. In the final analysis, sufficiency depends upon usage and availability of any better alternative data. TLEs may be more than adequate for less-demanding purposes. And despite disparaging comments about TLE accuracy, it is important to remember that SP orbit determination can be adversely impacted by its own set of accuracy degradations, errors, misassociations and issues.

Beyond utilizing the overall process shown in **Fig. 1** adopted here, this paper does not concern itself with implementation details of the Type 1 TLE fit process. But it is worth discussing the two Type 1 TLE fit papers in a bit more detail:

- **Cappellucci, SP to GP Extrapolated DC in Satellite Catalog Maintenance (AAS 05-402)**: This paper was one of the earlier versions of the Extrapolated Differential Correction (EDC) investigation, conducted by Lockheed Martin in 2005. The paper has good background information on how EDC might best be applied (to include discussions on pseudo-observation spacing, Sundmann transformation for elliptical orbits, fit spans, etc.). However, the paper doesn't contain much assessment of error metrics, and the few metrics it does contain are either notional (i.e. contains non-dimensional bar graphs) or sparse (e.g. ten satellite comparisons).
- **Hedjuk et al, Catalog-Wide Implementation of GP OD Extrapolated From Higher Order Orbital Theory (AAS 13-240):** Examines the ability of EGP TLEs to match SP ephemerides. The AAS 13-240 paper is the most similar to this current AGI study. The authors found similar difficulties in lower LEO application of EGP as will be demonstrated in the following sections.

In contrast to the research of papers AAS 05-402 and AAS 13-240, this study differs in the following key respects:

- The authors' goal of AAS 05-402 and AAS 13-240 was not to show that the EGP TLEs match reality better than prior TLEs, but rather to show that the EGP TLEs are sufficiently within family of the underlying SP vectors and ephemerides upon which the EGP TLEs are based;
- The authors used SP "reference orbits" as truth, perhaps clouding the issue of how well EGP fits actual orbits because SP reference orbits are pieced together sequences of SP ephemerides, each of which could have accuracy degradations of their own – observational undersampling, unmodeled maneuvers, track misassociation, space weather dynamics, unmodeled or mismodeled perturbations;
- The authors only reported median error for a few orbit types as opposed to the 150 orbit altitude/inclination combinations examined here;
- The authors did not provide the wealth of Vmag, Radial, In-Track and Cross-Track error characterizations and statistics (median, mean, skewness, deviations, percentiles, minimum, maximum and Gaussian-ness) as provided here.

5. ANALYSIS APPROACH

Differences between SGP4 Semi-Analytic Theory (upon which TLEs are based) and detailed numerical integration (SP) are too numerous and complex to analytically quantify. To conduct this analysis, we instead avoid these complexities by simulating our own idealized "truth orbits" to see how well "EGP TLEs" fit them (**Fig. 2**.)

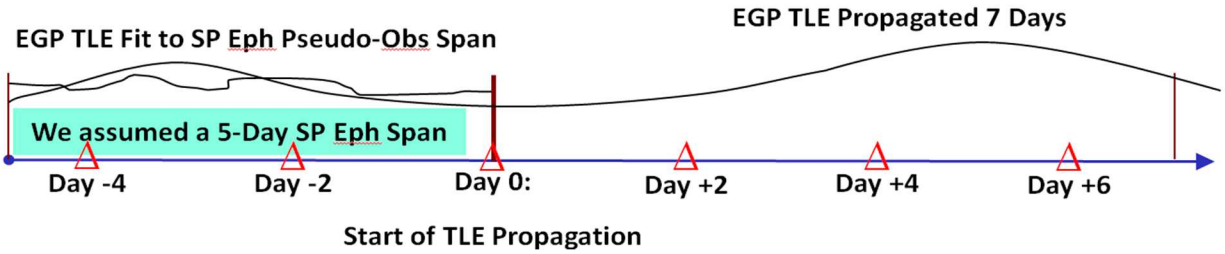

Fig. 2: Truth orbit and EGP fit process adopted for this study

For this study, twelve days of numerically-integrated "truth" orbits and associated pseudo-observations were generated. Parametric cases spanned variations in orbit altitude (from 350 km up to geosynchronous earth orbit), orbit inclination (median, 1σ-high and 1σ-low values at each orbit altitude[8] as shown in **Fig. 3** and **Fig. 4**) and right ascension of the ascending node (sampled in 90° increments from 0° to 360°). Altitude step size was 50 km from 350 to 750 km (large errors observed below 320 km) and 250 km from 900 to 35650 km.

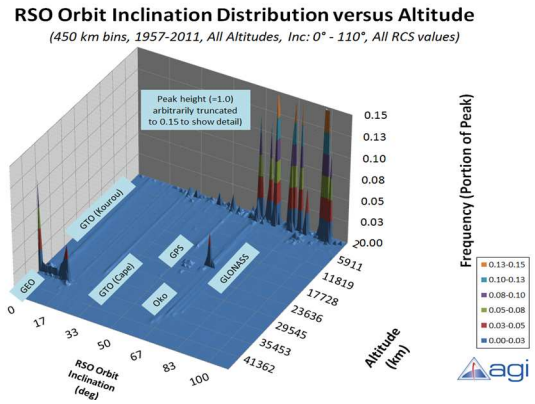

Fig. 3: Orbit inclination distribution by altitude

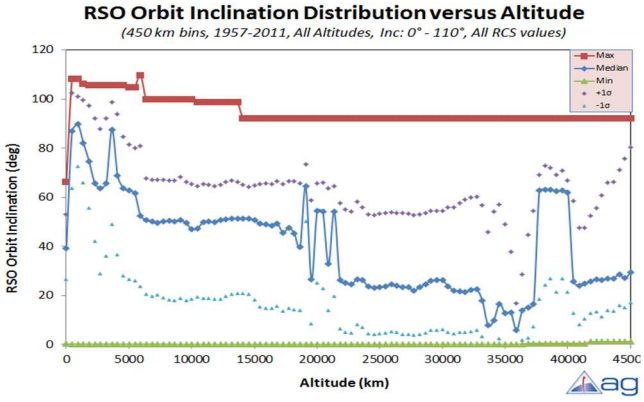

Fig. 4: Orbit inclination distrib. statistics by altitude

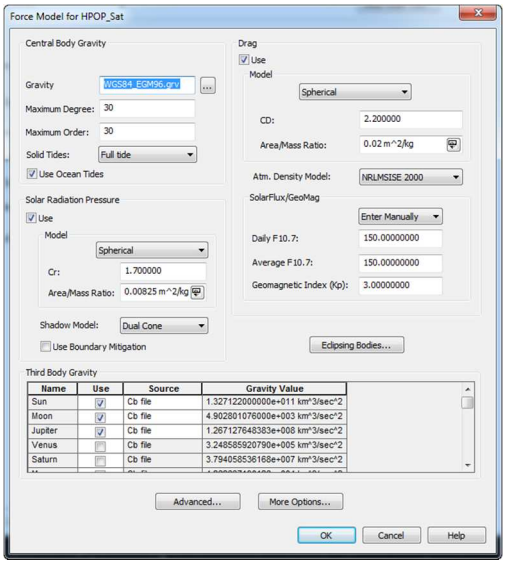

Fig. 5: HPOP force model control settings

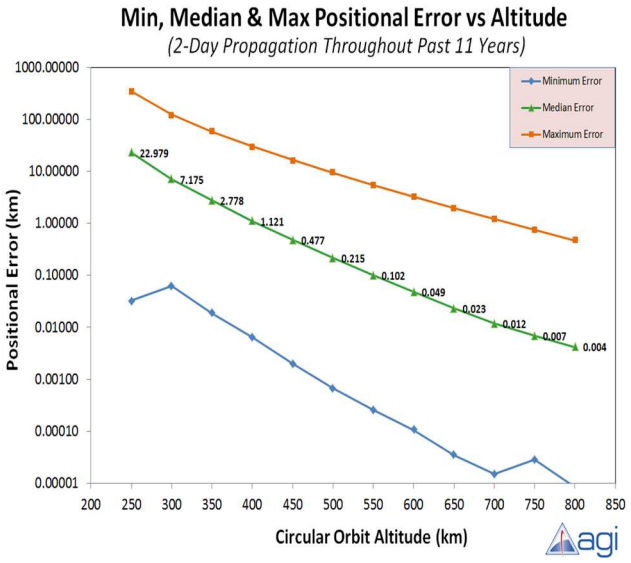

Fig. 6: Impact of space weather uncertainties to orbit propagation

Note that at all altitudes, only circular orbits were considered. STK HPOP was used to create truth orbits with a full force model, including EGM-96 30 x 30 gravity model, drag (Cd=2.2, Area-to-mass= 0.02 m^2/kg), SRP (Cr=1.7, Area-to-mass=0.00825 m^2/kg), Sun, Moon, and Jupiter 3rd-Body, and full solid & ocean tide perturbations (**Fig. 5**).

Note also that fixed space weather (F10=F10.7=150, Kp=3) was arbitrarily assumed for this study. Space weather yields additional uncertainties to both SP and TLEs. For example, **Fig. 6** was created by parametrically sampling through an entire solar cycle the difference between a truth orbit propagation of 2 days using actual space weather data versus holding space weather extant at the propagation start time constant throughout the two days.

For each of the parametric combinations listed above, TLEs were fit to the first 5 days of the HPOP truth orbits with an epoch set to the end of the 5-day fit span (heretofore referred to as "Day 0". These "EGP" TLEs were then propagated -5 to +7 days from the "Day 0" epoch to provide direct overlap between the original truth ephemeris and the EGP TLE-derived ephemeris. Error PDFs in positional knowledge (vector magnitude RSS as well as radial, in-track and cross-track components) were then accumulated at a Δ time step size of 15 seconds. The median inclination statistics were weighted accordingly higher than the $\pm 1\sigma$ cases.

6. RESULTS AND CONCLUSIONS

Positional difference PDFs and statistical are now provided for comparisons of EGP TLEs with respect to the HPOP truth ephemerides as captured at epochs of -4, -2, 0, 2, 4 and 6 days from "Day 0" (with +days denoting times after "Day 0". Statistics include the 4.6% and 95.4% percentiles, median (typical) difference, minimum and maximum difference, as well as standard deviation, skewness, kurtosis and Jarque-Bera metrics.

6.1 General Observations and Conclusions

The figures show that the EGP fit process (and by extension the underlying SGP4 theory) typically performs to better than 1 km across the entire orbit altitude range from 350 km to geosynchronous orbit altitude. Interestingly, a noticeable "hiccup" in EGP TLE accuracy is commonly found for altitudes neighboring the 8-hour orbital period (resonance=3) mark in all comparison cases. Fortunately, examination of spatial density for 8-hour orbits reveals that there are very few objects inhabiting this regime. The 225-minute orbital period break-point between the GP "LEO" theory and that of "Deep Space" is also readily apparent in the plots (*e.g.,* **Fig. 22** and **Fig. 23**).

Historically, large discrepancies have been observed between published TLEs and ephemerides of many positionally-well-known satellites (WAAS, laser calibration spheres, GPS, and owner/operator satellites). These discrepancies have often exceeded the parametrically-characterized performance of EGP TLEs ten- or even twenty-fold. This is not an unexpected result, when one it considers the components of error that exist in a non-cooperative tracking system. In addition to lower-fidelity orbit modeling (e.g. GP theory), these include the lack of maneuver information and accommodation for active satellites within the current batch least-squares orbit determination (OD) process, the potential for undersampling of OD observations due to dependence on optical sensors (e.g. in GEO, where only half of a satellite's orbit is typically observed), the presence of track mis-association and cross tagging, and other significant effects. For example, at 400 km, note from **Fig. 6** that the analyst will typically experience $Error_{SpaceWx} = 1.121\ km$ of error solely due to our inability to predict space weather, whereas for that same 400 km altitude, $Error_{Low-Fidelity\ Orbit\ Modeling}$ (the error introduced by using EGP TLEs instead of an SP orbit) is less than 1 km (850 meters).

In equation form:

$$Error_{Total} = Error_{Maneuvers} + Error_{Undersampling} + Error_{Cross-tags} + Error_{SpaceWx} + Error_{Low-Fidelity\ Orbit\ Modeling} + Error_{Improper\ Sensor\ Calibration} + \cdots \quad (1)$$

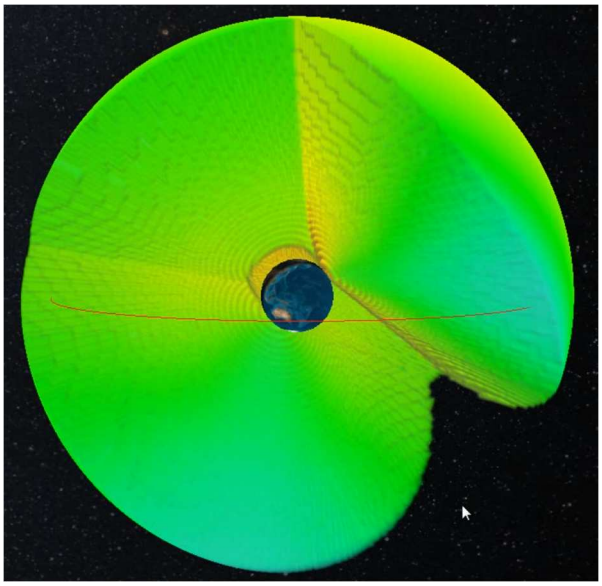

Fig. 7: Cyclical positional error profile due to undersampling (minimal GEO coverage on solar-illuminated side of Earth)

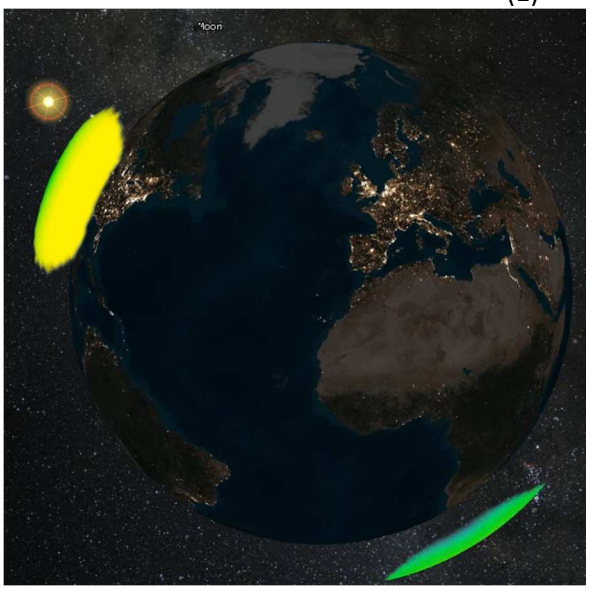

Fig. 8: Even further undersampled case of optical coverage for LEO (requires radar augmentation to maintain accuracy and custody)

6.2 Day -4: EGP TLE Parametric Fit Performance

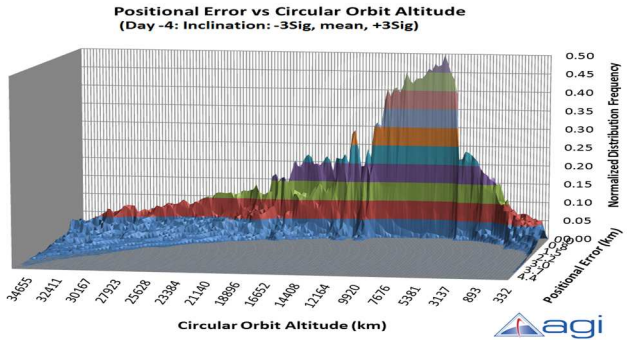

Fig. 9: Day -4: Positional error PDF =f(altitude)

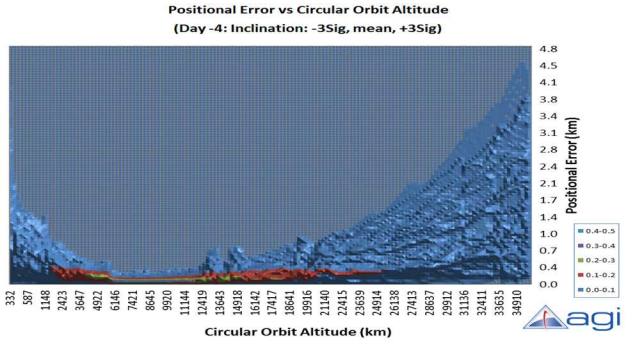

Fig. 10: Day -4: Positional error PDF =f(altitude)

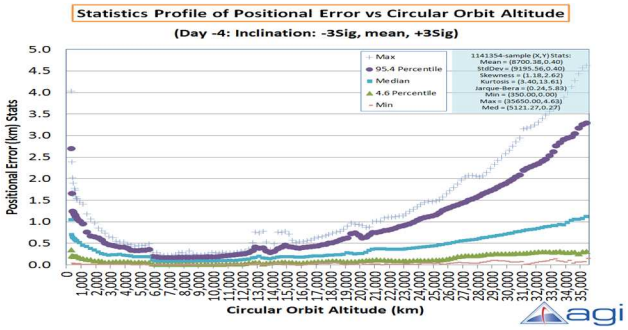

Fig. 11: Day -4: Positional error statistics

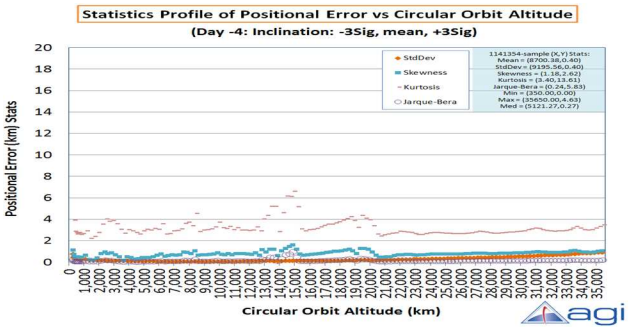

Fig. 12: Day -4: Positional error skewness, kurtosis

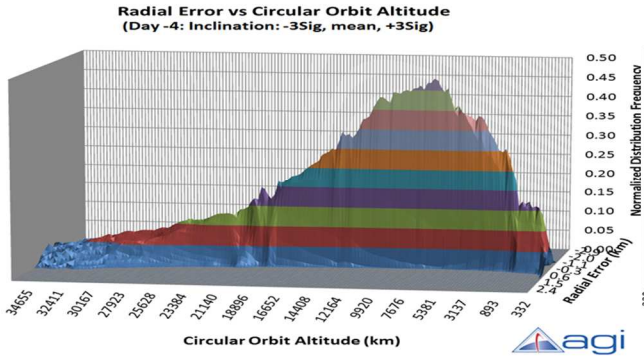

Fig. 13: Day -4: Radial error PDF =f(altitude)

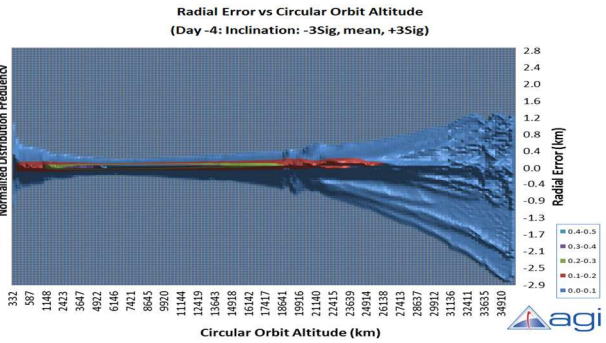

Fig. 14: Day -4: Radial error PDF =f(altitude)

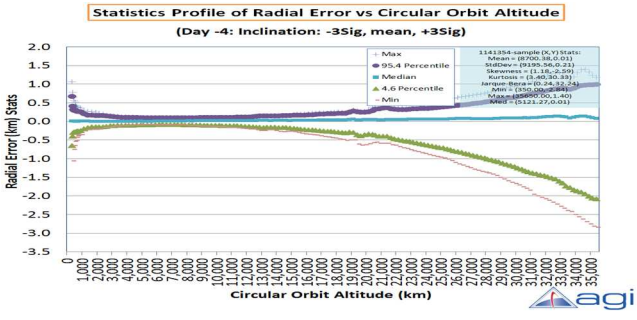

Fig. 15: Day -4: Radial error statistics

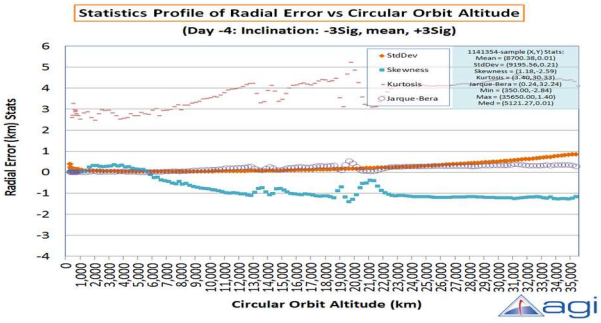

Fig. 16: Day -4: Radial error skewness, kurtosis

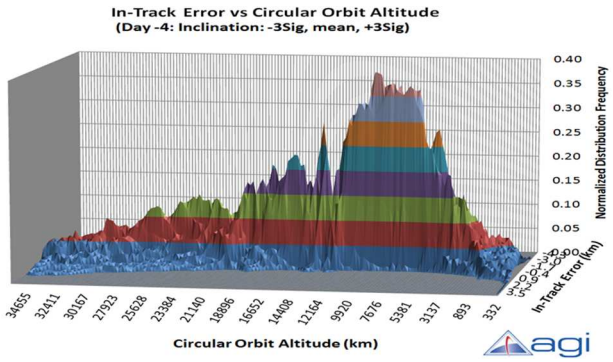

Fig. 17: Day -4: In-track error PDF =f(altitude)

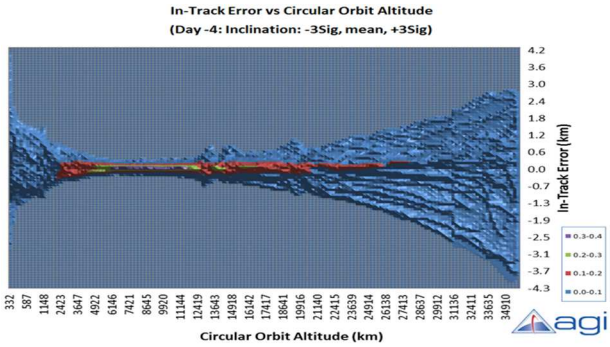

Fig. 18: Day -4: In-track error PDF =f(altitude)

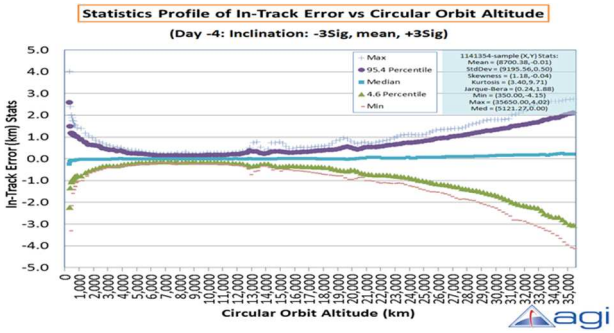

Fig. 19: Day -4: In-track error statistics

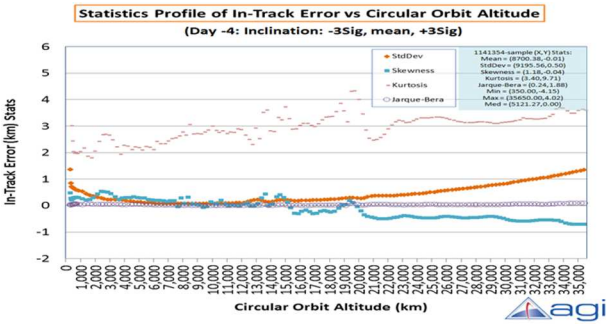

Fig. 20: Day -4: In-track error skewness, kurtosis

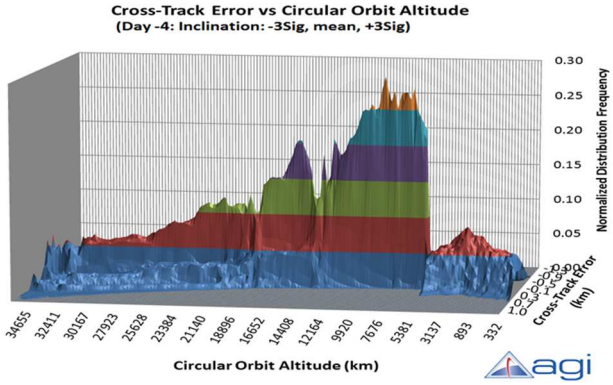

Fig. 21: Day -4: Cross-track error PDF =f(altitude)

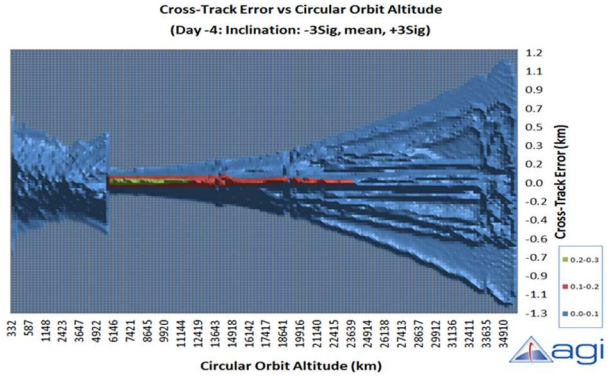

Fig. 22: Day -4: Cross-track error statistics

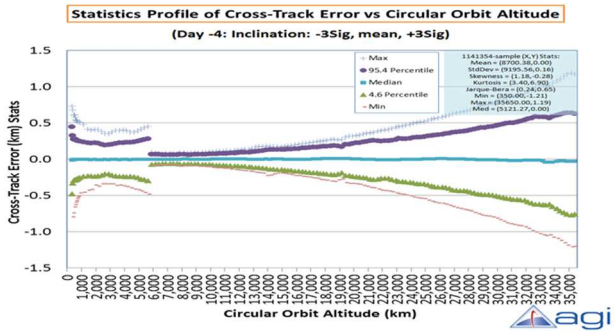

Fig. 23: Day -4: Cross-track error statistics

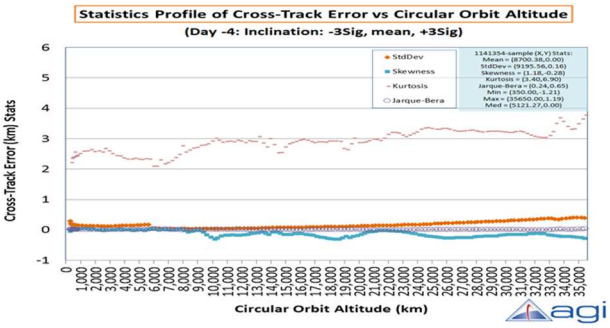

Fig. 24: Day -4: Cross-track error skewness, kurtosis

6.3 Day -2: EGP TLE Parametric Fit Performance

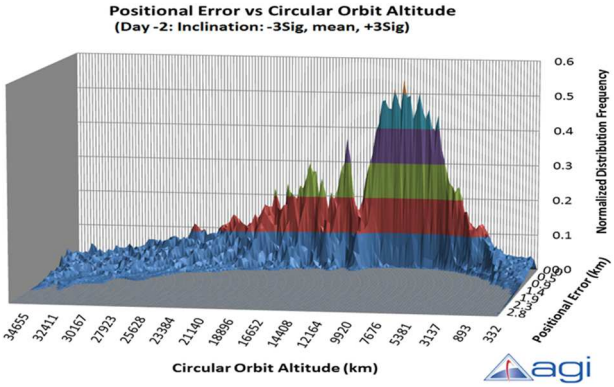

Fig. 25: Day -2: Positional error PDF =f(altitude)

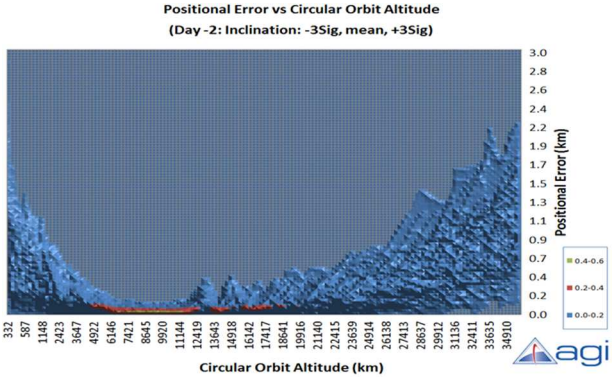

Fig. 26: Day -2: Positional error PDF =f(altitude)

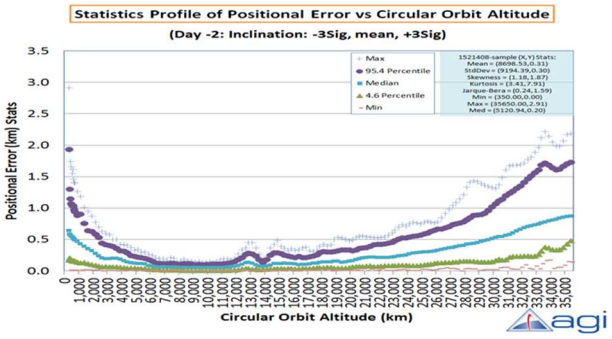

Fig. 27: Day -2: Positional error statistics

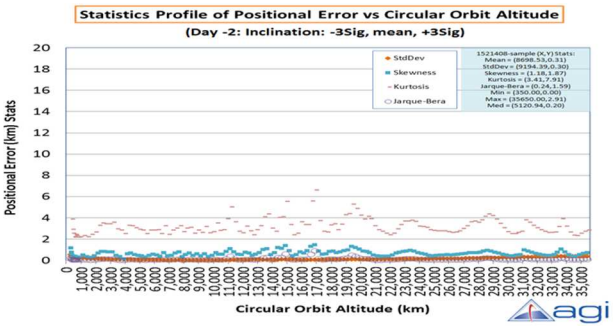

Fig. 28: Day -2: Positional error skewness, kurtosis

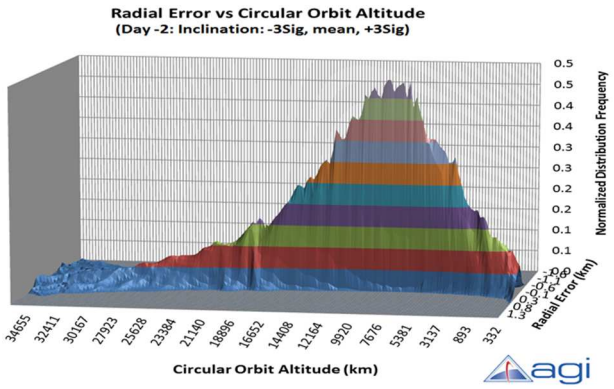

Fig. 29: Day -2: Radial error PDF =f(altitude)

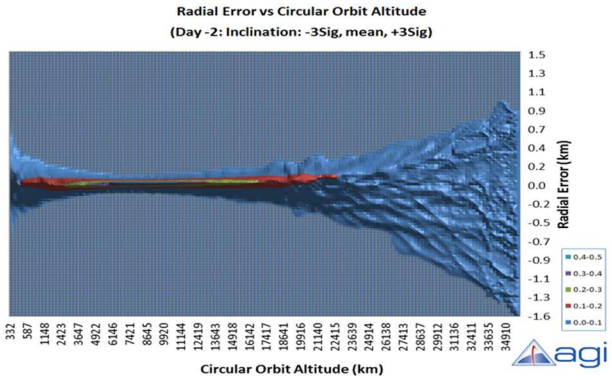

Fig. 30: Day -2: Radial error PDF =f(altitude)

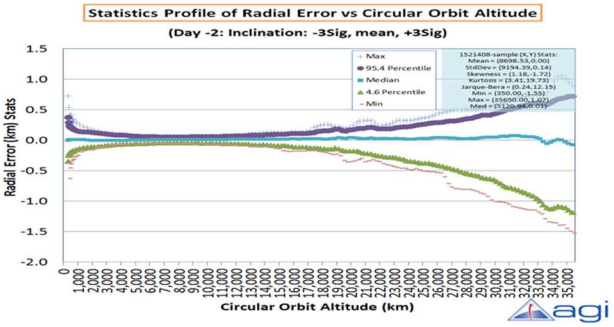

Fig. 31: Day -2: Radial error statistics

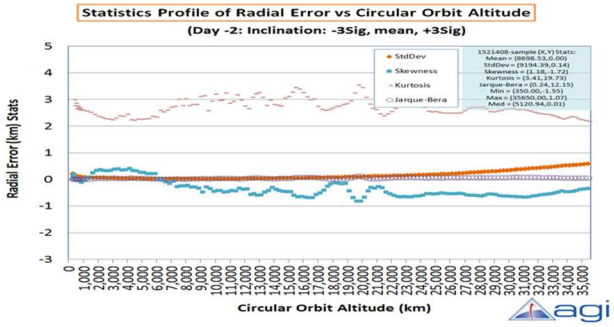

Fig. 32: Day -2: Radial error skewness, kurtosis

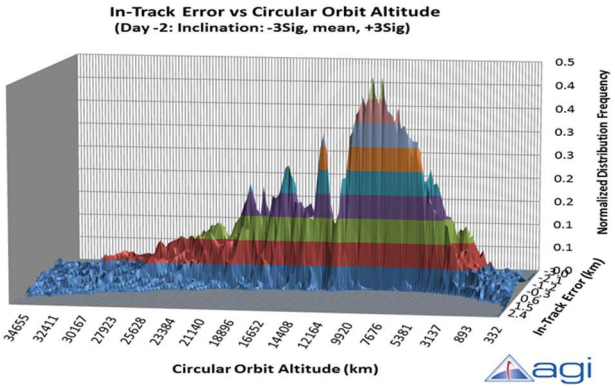

Fig. 33: Day -2: In-track error PDF =f(altitude)

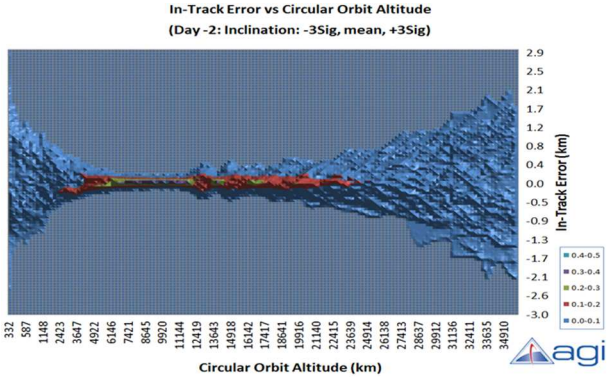

Fig. 34: Day -2: In-track error PDF =f(altitude)

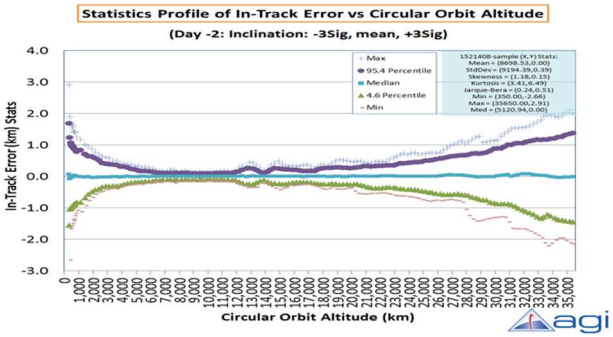

Fig. 35: Day -2: In-track error statistics

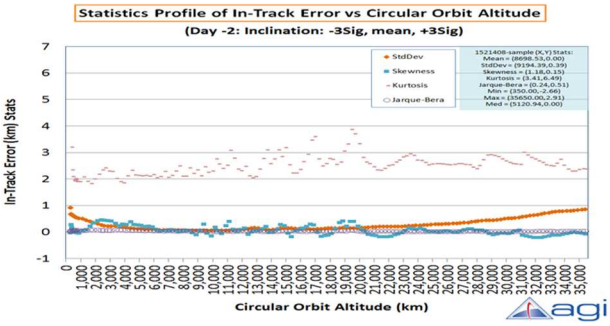

Fig. 36: Day -2: In-track error skewness, kurtosis

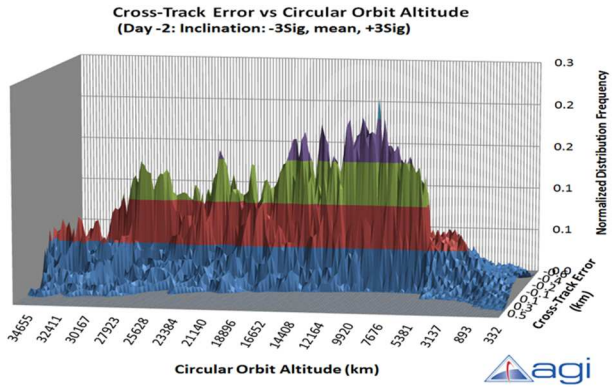

Fig. 37: Day -2: Cross-track error PDF =f(altitude)

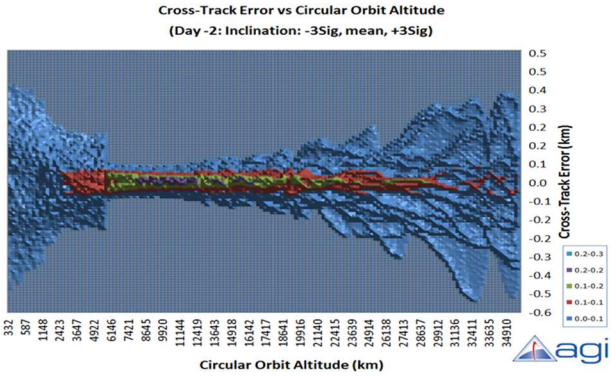

Fig. 38: Day -2: Cross-track error statistics

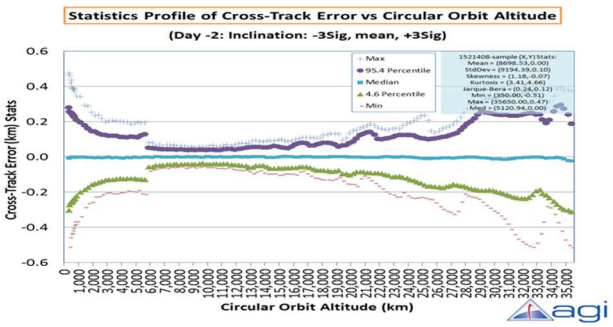

Fig. 39: Day -2: Cross-track error statistics

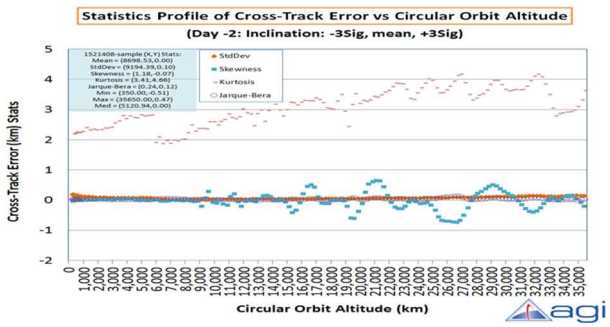

Fig. 40: Day -2: Cross-track error skewness, kurtosis

6.4 Day 0: EGP TLE Parametric Fit Performance

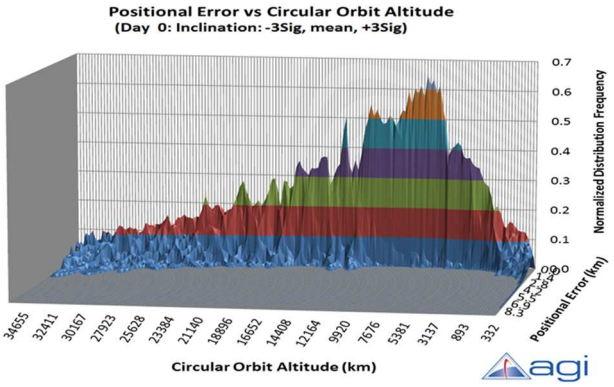

Fig. 41: Day 0: Positional error PDF =f(altitude)

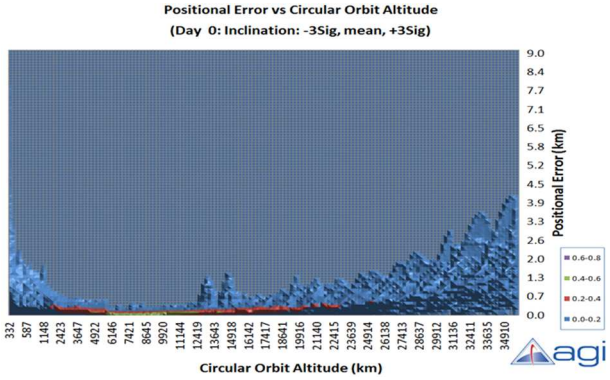

Fig. 42: Day 0: Positional error PDF =f(altitude)

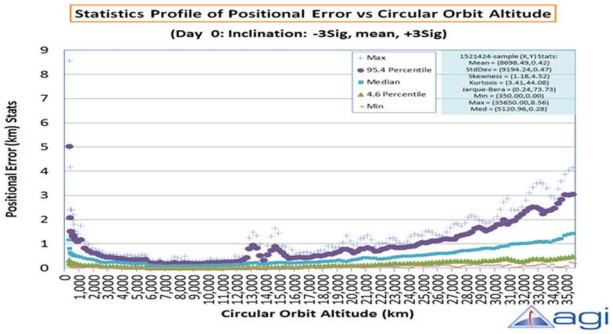

Fig. 43: Day 0: Positional error statistics

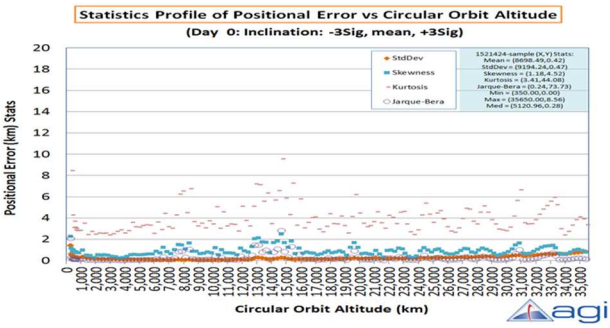

Fig. 44: Day 0: Positional error skewness, kurtosis

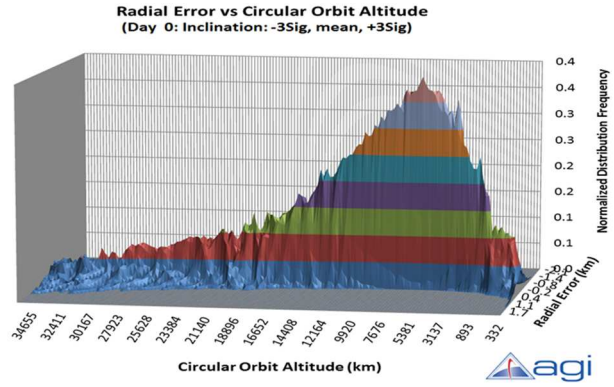

Fig. 45: Day 0: Radial error PDF =f(altitude)

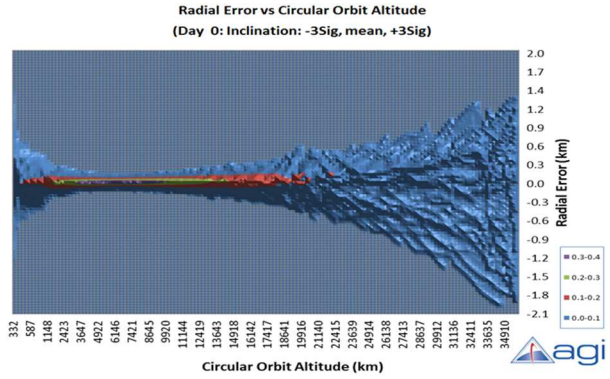

Fig. 46: Day 0: Radial error PDF =f(altitude)

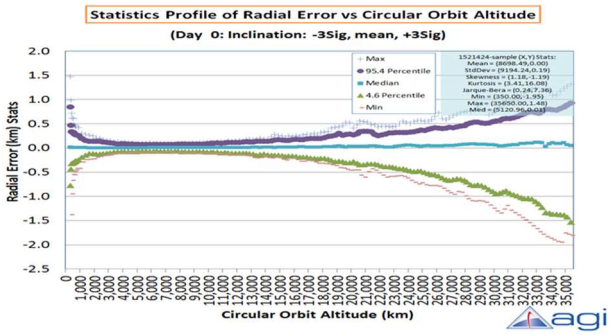

Fig. 47: Day 0: Radial error statistics

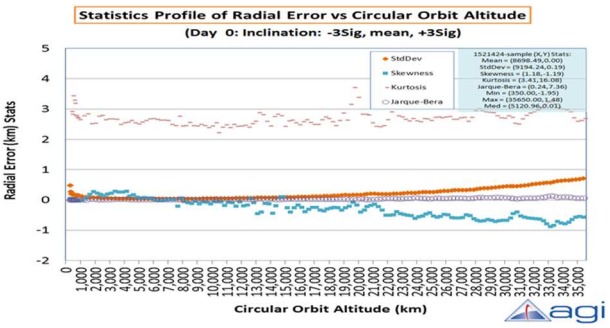

Fig. 48: Day 0: Radial error skewness, kurtosis

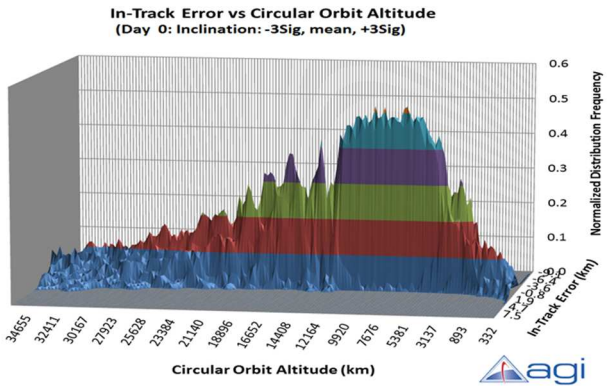

Fig. 49: Day 0: In-track error PDF =f(altitude)

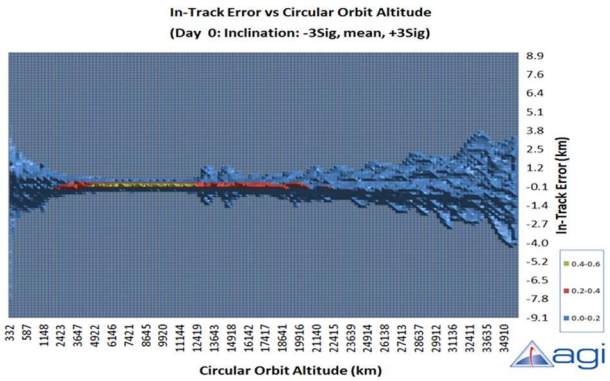

Fig. 50: Day 0: In-track error PDF =f(altitude)

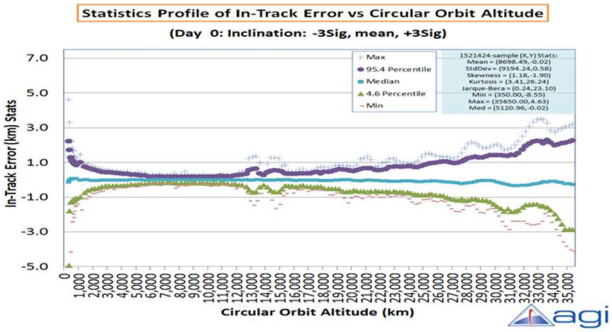

Fig. 51: Day 0: In-track error statistics

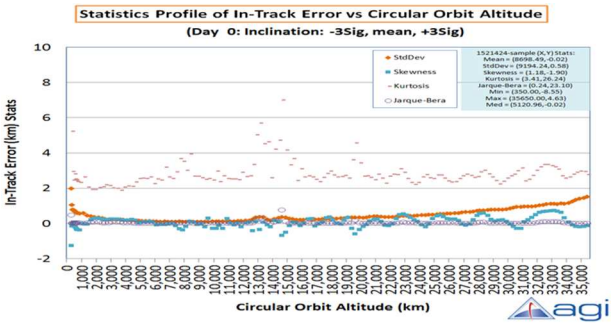

Fig. 52: Day 0: In-track error skewness, kurtosis

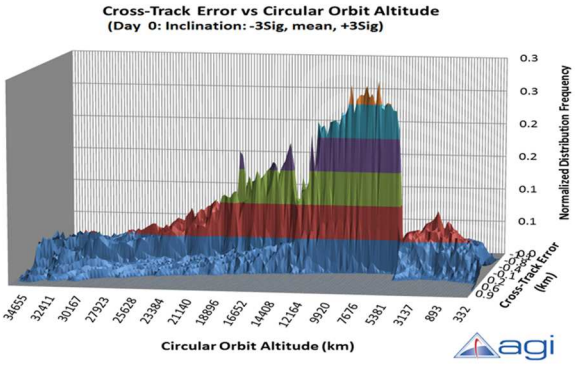

Fig. 53: Day 0: Cross-track error PDF =f(altitude)

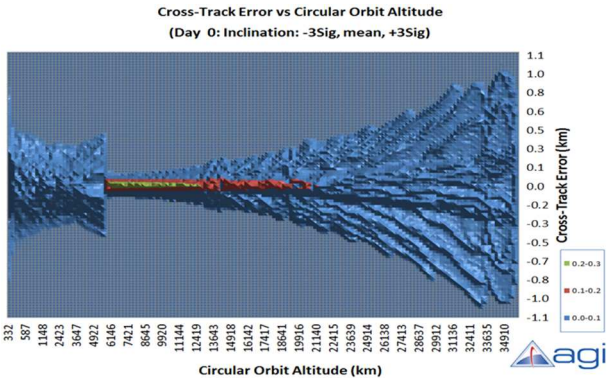

Fig. 54: Day 0: Cross-track error statistics

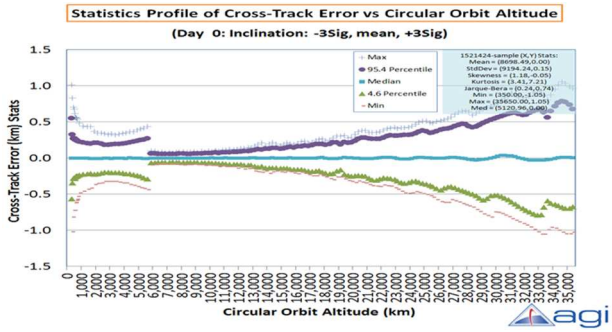

Fig. 55: Day 0: Cross-track error statistics

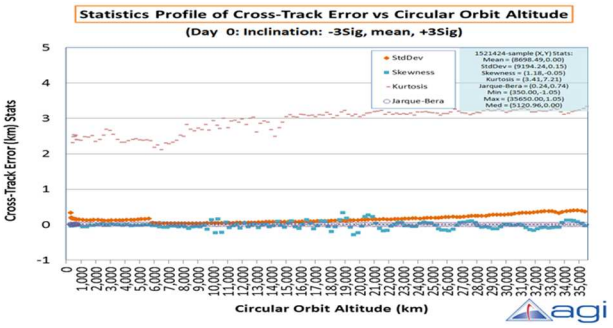

Fig. 56: Day 0: Cross-track error skewness, kurtosis

6.5 Day +2: EGP TLE Parametric Fit Performance

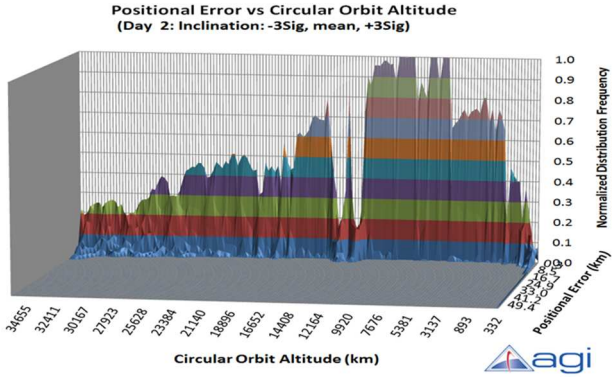

Fig. 57: Day +2: Positional error PDF =f(altitude)

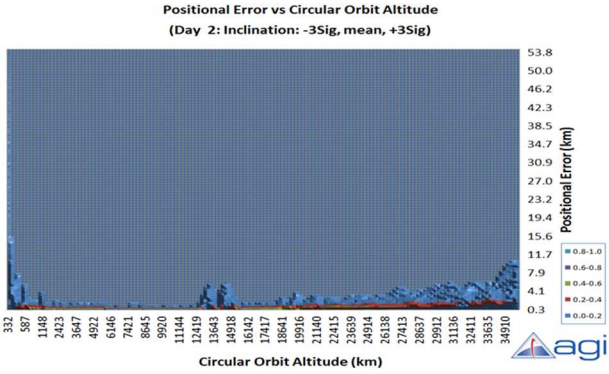

Fig. 58: Day +2: Positional error PDF =f(altitude)

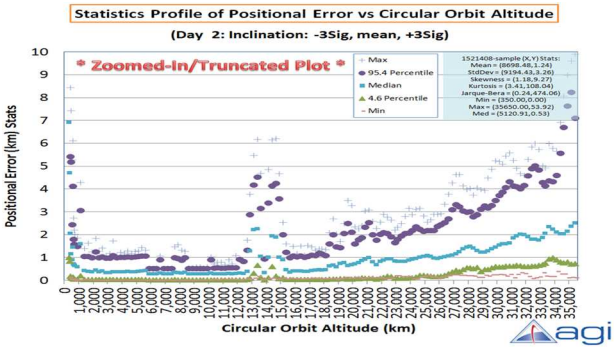

Fig. 59: Day +2: Positional error statistics

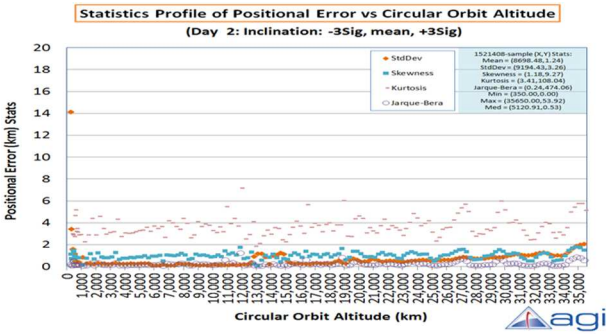

Fig. 60: Day +2: Positional error skewness, kurtosis

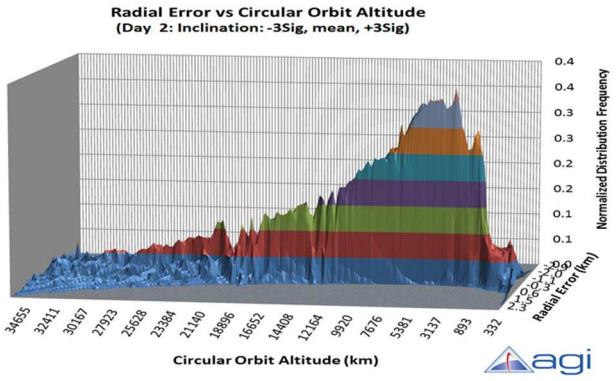

Fig. 61: Day +2: Radial error PDF =f(altitude)

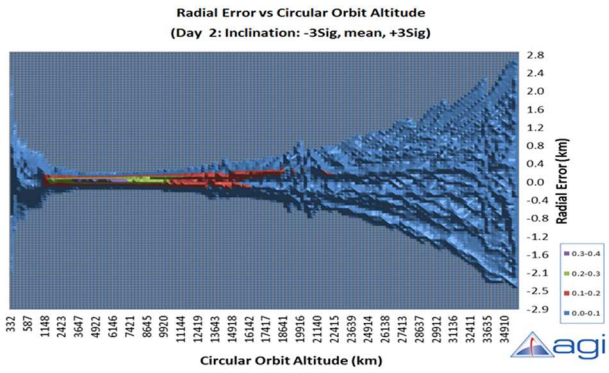

Fig. 62: Day +2: Radial error PDF =f(altitude)

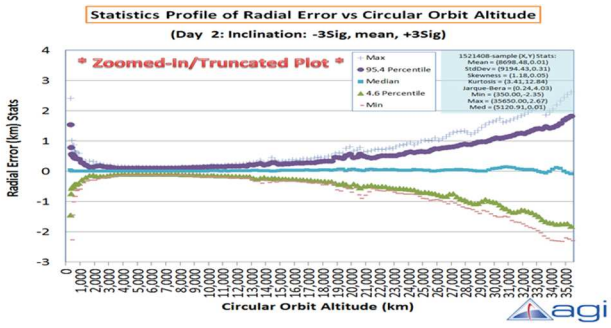

Fig. 63: Day +2: Radial error statistics

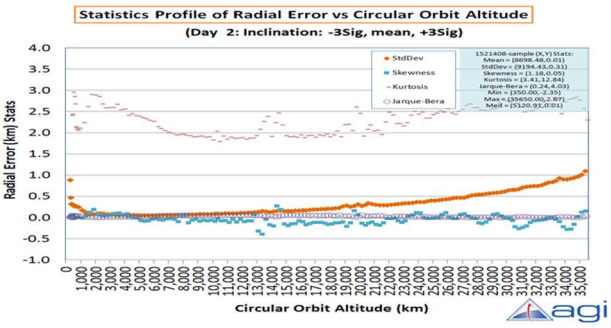

Fig. 64: Day +2: Radial error skewness, kurtosis

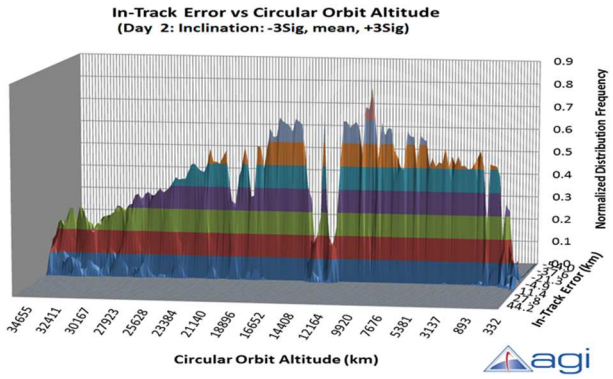

Fig. 65: Day +2: In-track error PDF =f(altitude)

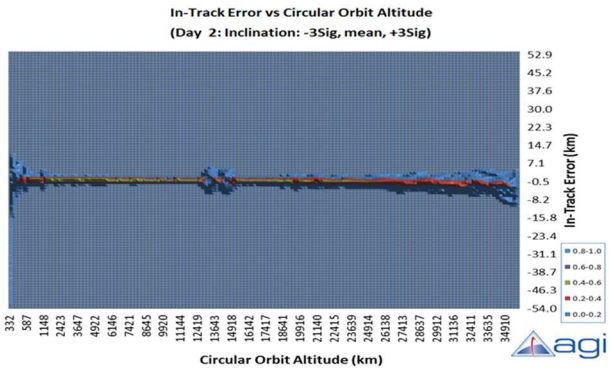

Fig. 66: Day +2: In-track error PDF =f(altitude)

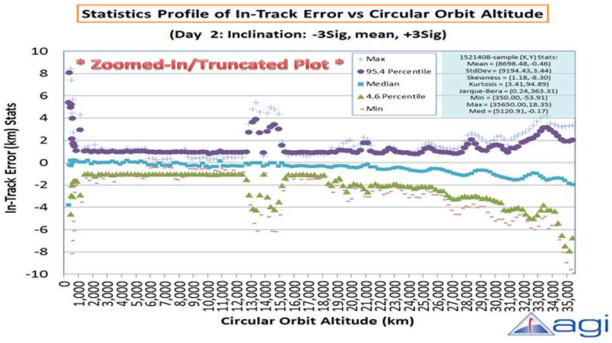

Fig. 67: Day +2: In-track error statistics

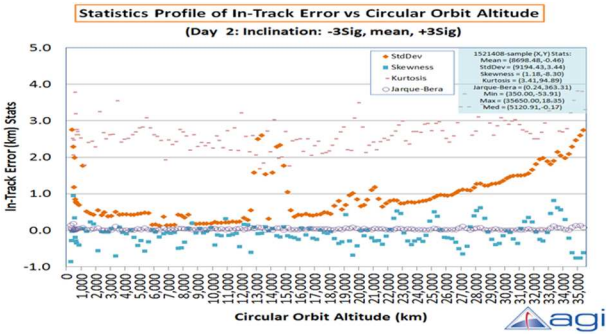

Fig. 68: Day +2: In-track error skewness, kurtosis

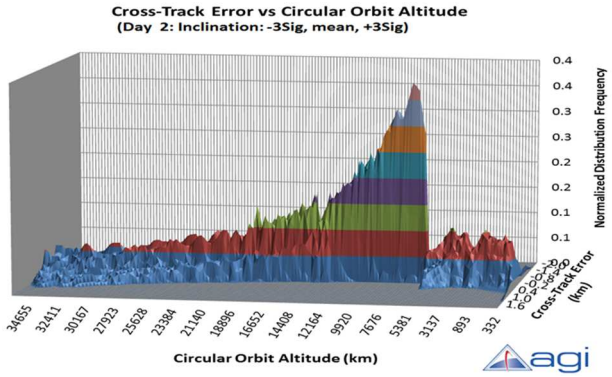

Fig. 69: Day +2: Cross-track error PDF =f(altitude)

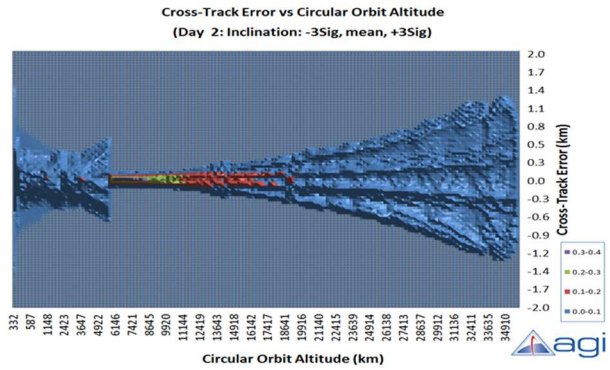

Fig. 70: Day +2: Cross-track error statistics

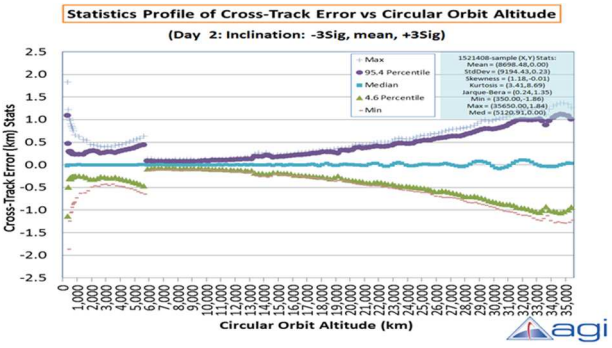

Fig. 71: Day +2: Cross-track error statistics

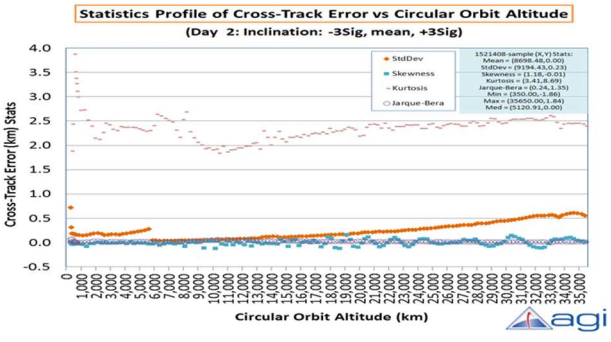

Fig. 72: Day +2: Cross-track error skewness, kurtosis

6.6 Day +4: EGP TLE Parametric Fit Performance

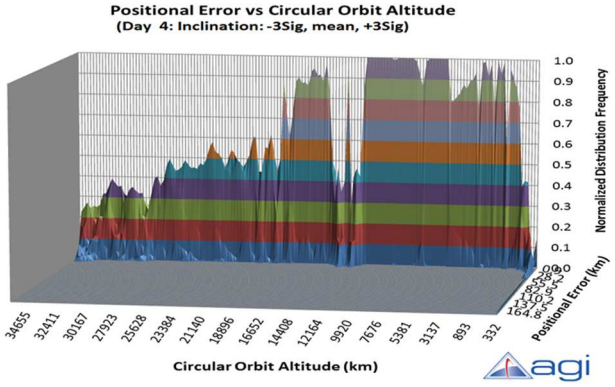

Fig. 73: Day +4: Positional error PDF =f(altitude)

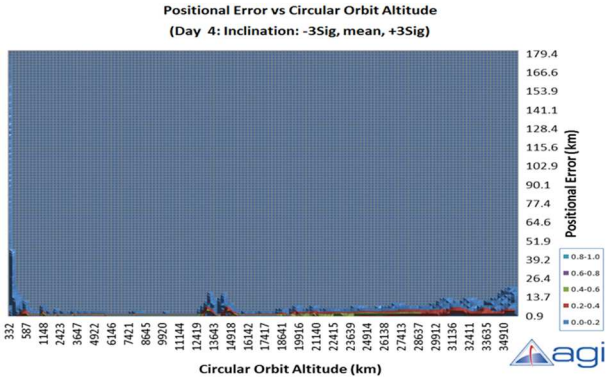

Fig. 74: Day +4: Positional error PDF =f(altitude)

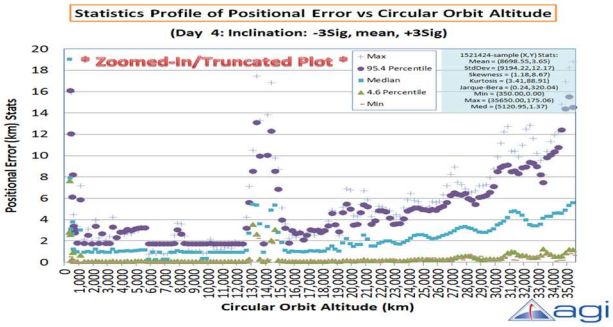

Fig. 75: Day +4: Positional error statistics

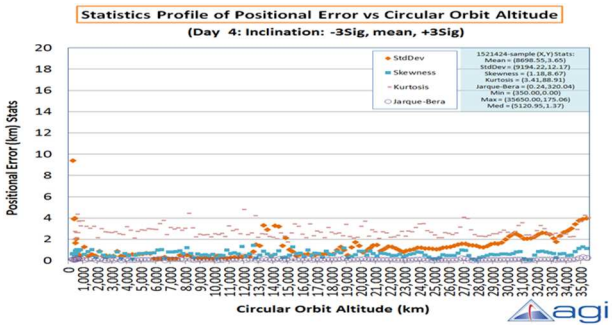

Fig. 76: Day +4: Positional error skewness, kurtosis

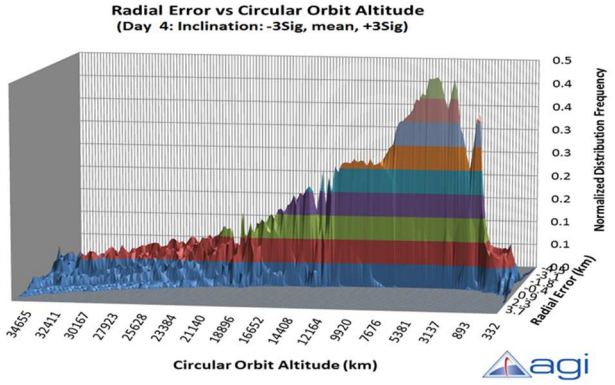

Fig. 77: Day +4: Radial error PDF =f(altitude)

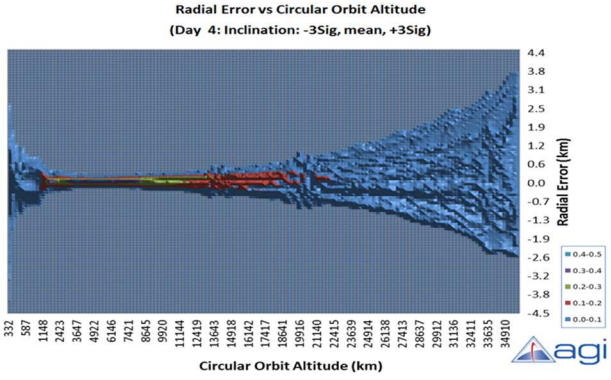

Fig. 78: Day +4: Radial error PDF =f(altitude)

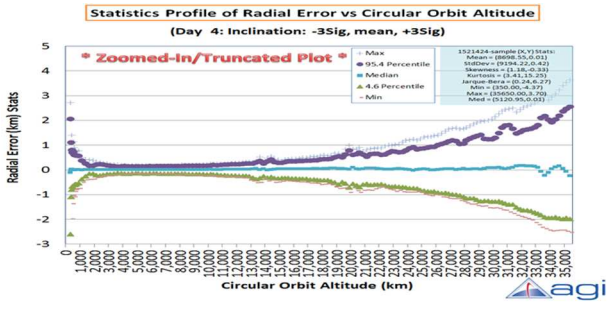

Fig. 79: Day +4: Radial error statistics

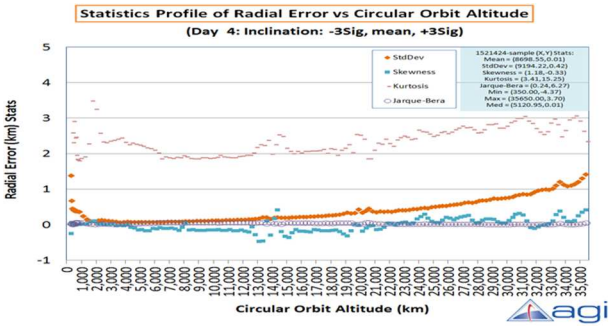

Fig. 80: Day +4: Radial error skewness, kurtosis

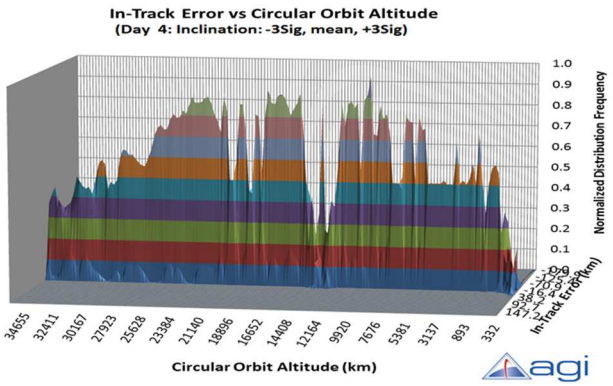

Fig. 81: Day +4: In-track error PDF =f(altitude)

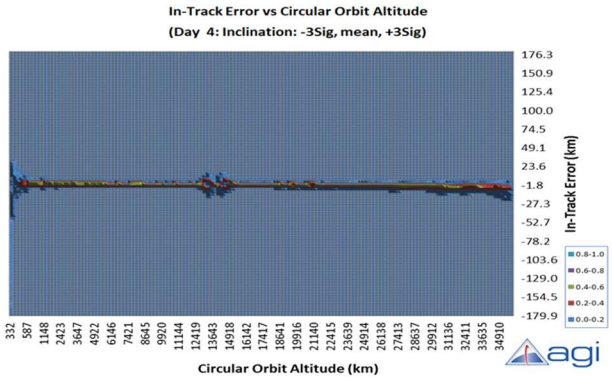

Fig. 82: Day +4: In-track error PDF =f(altitude)

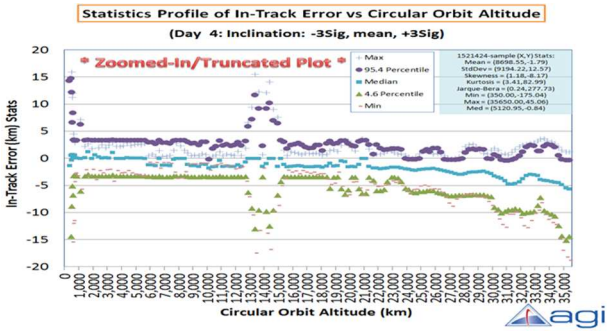

Fig. 83: Day +4: In-track error statistics

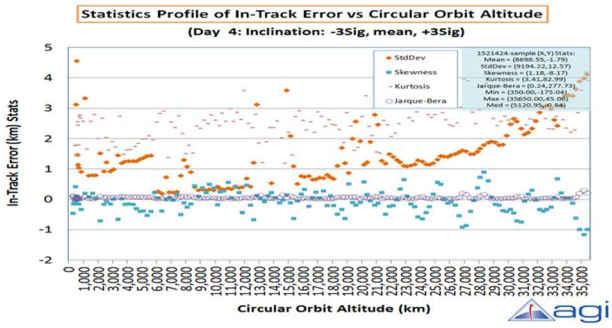

Fig. 84: Day +4: In-track error skewness, kurtosis

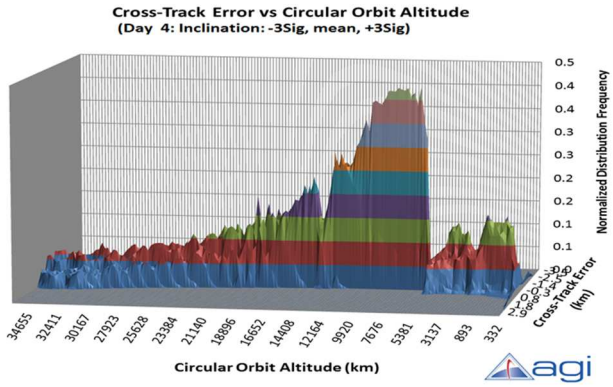

Fig. 85: Day +4: Cross-track error PDF =f(altitude)

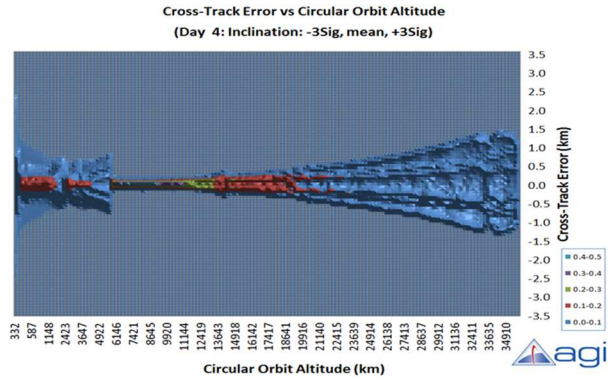

Fig. 86: Day +4: Cross-track error statistics

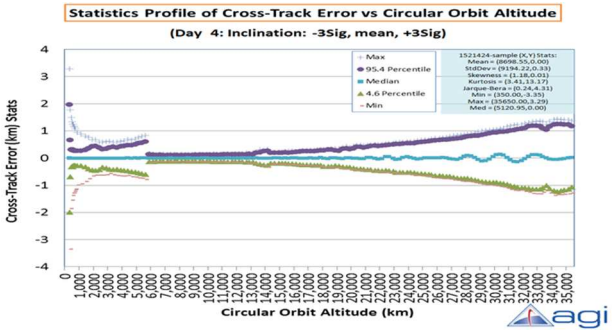

Fig. 87: Day +4: Cross-track error statistics

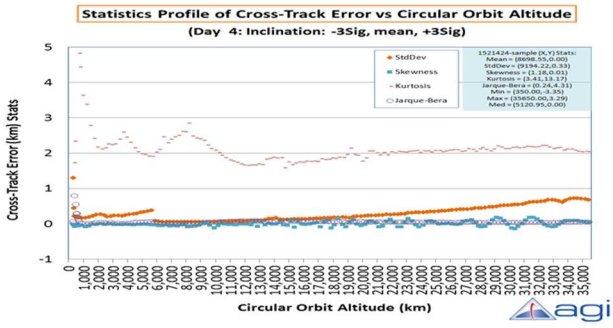

Fig. 88: Day +4: Cross-track error skewness, kurtosis

6.7 Day +6: EGP TLE Parametric Fit Performance

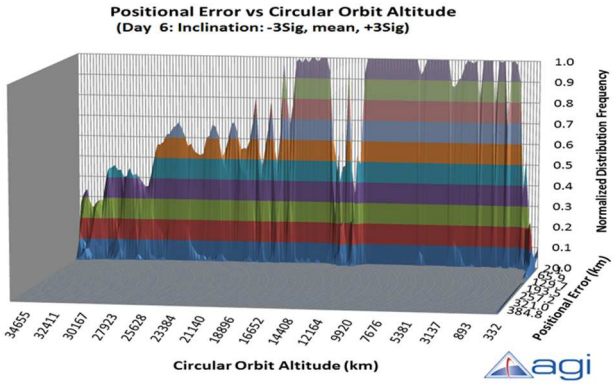

Fig. 89: Day +6: Positional error PDF =f(altitude)

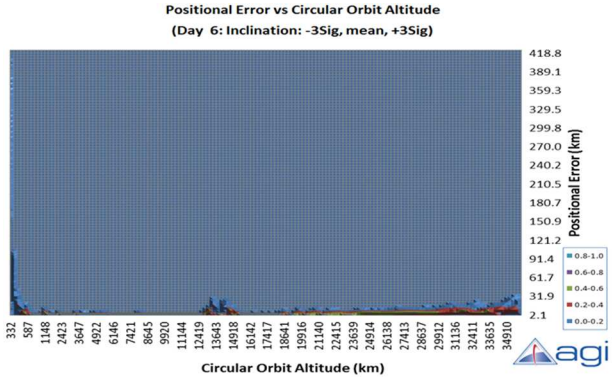

Fig. 90: Day +6: Positional error PDF =f(altitude)

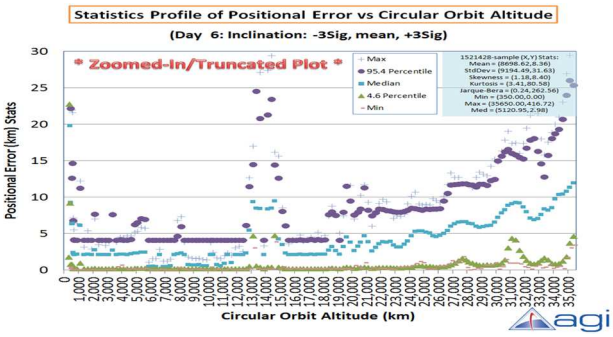

Fig. 91: Day +6: Positional error statistics

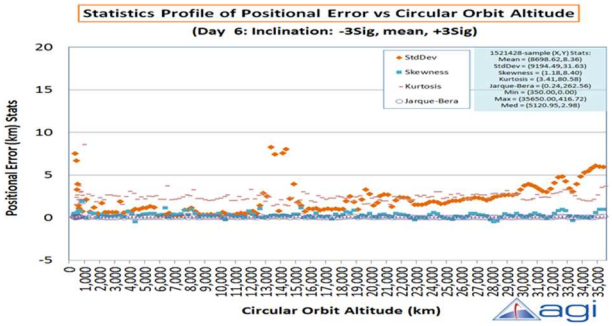

Fig. 92: Day +6: Positional error skewness, kurtosis

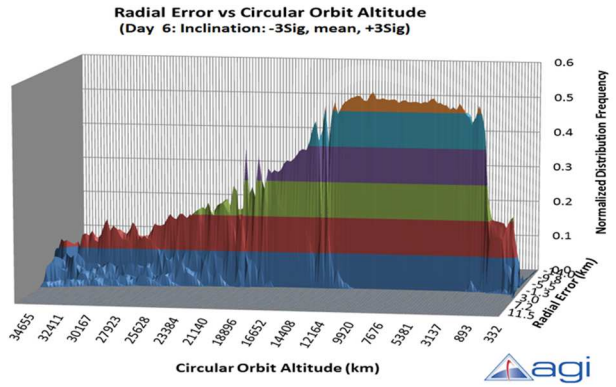

Fig. 93: Day +6: Radial error PDF =f(altitude)

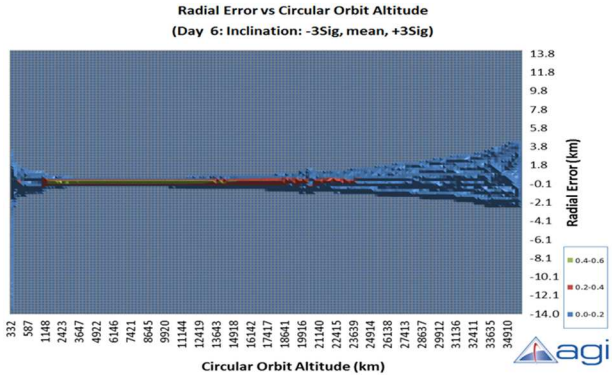

Fig. 94: Day +6: Radial error PDF =f(altitude)

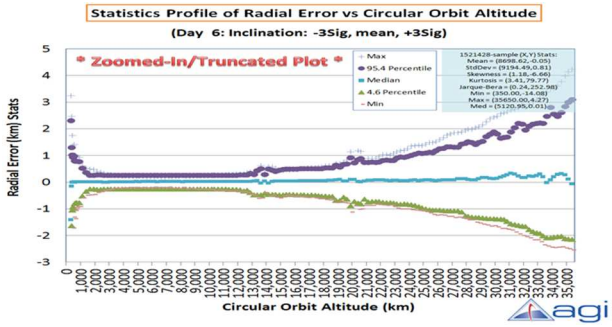

Fig. 95: Day +6: Radial error statistics

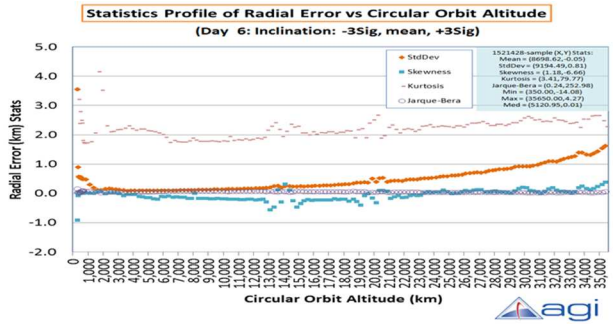

Fig. 96: Day +6: Radial error skewness, kurtosis

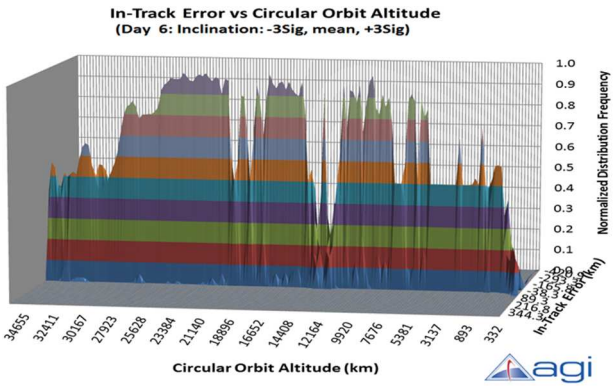

Fig. 97: Day +6: In-track error PDF =f(altitude)

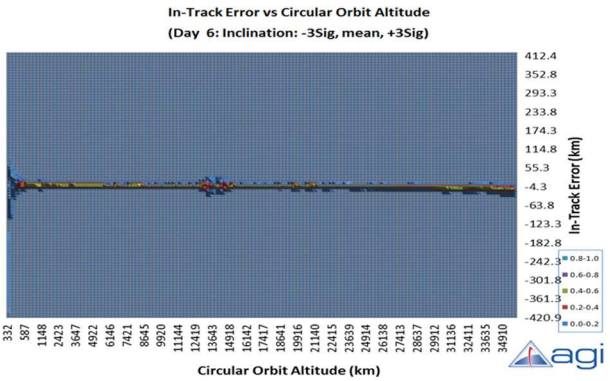

Fig. 98: Day +6: In-track error PDF =f(altitude)

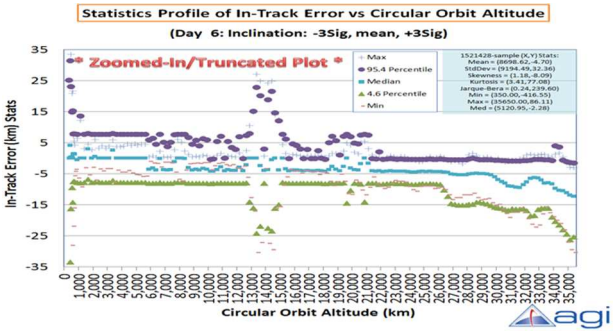

Fig. 99: Day +6: In-track error statistics

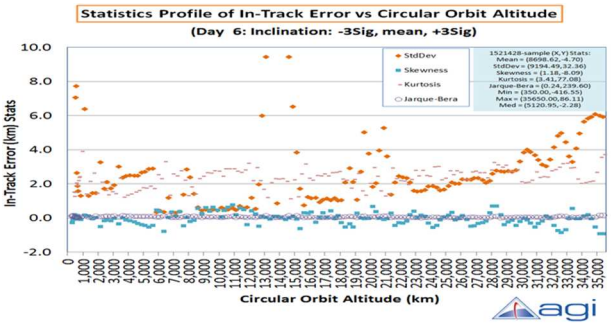

Fig. 100: Day +6: In-track error skewness, kurtosis

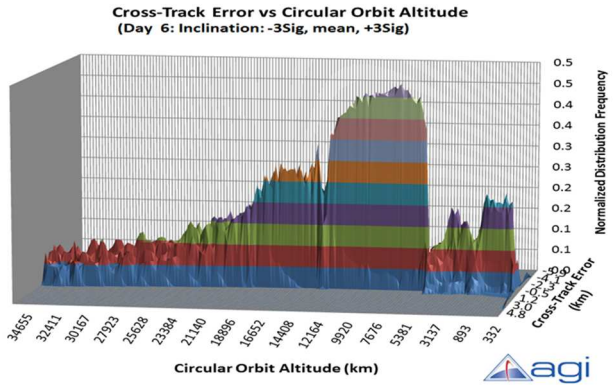

Fig. 101: Day +6: Cross-track error PDF =f(altitude)

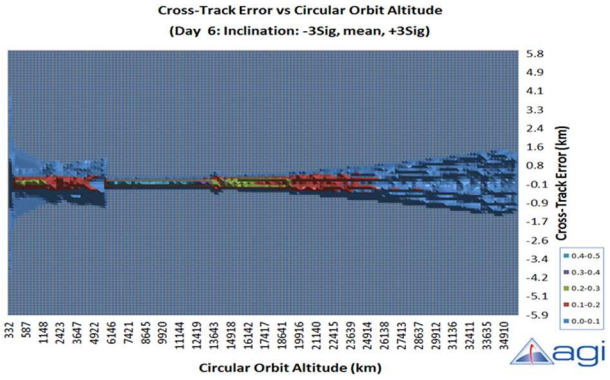

Fig. 102: Day +6: Cross-track error statistics

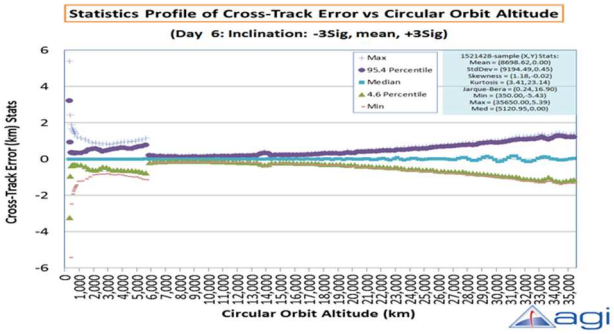

Fig. 103: Day +6: Cross-track error statistics

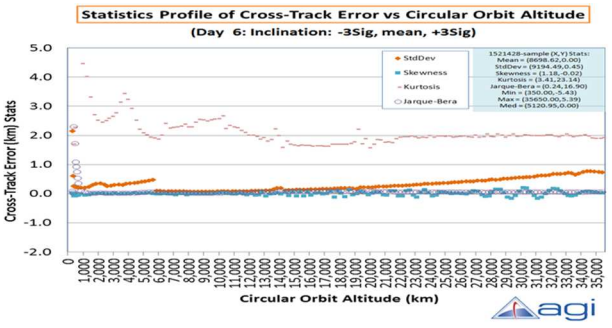

Fig. 104: Day +6: Cross-track skewness, kurtosis

7. References

[1] Cappellucci, D.A., "Special Perturbations to General Perturbations Extrapolation Differential Corrections in Satellite Catalog Maintenance, AAS 05-402.
[2] Hejduk et al, "A Catalog-Wide Implementation of General Perturbations Orbit Determination Extrapolated From Higher Order Orbital Theory Solutions," AAS 13-240, Spaceflight Mechanics Conference, Kauai, HI 2013
[3] Fundamentals of Astrodynamics and Applications 4th Edition, Vallado, David A. 2007, Microcosm, Hawthorne, CA.
[4] Vallado, D.A. and Cefola, P.J., "Two-Line Element Sets – Practice and Use," IAC-12-A6.6.11.
[5] Vallado, D.A., Virgili, B.B., and Flohrer, T., "Improved SSA Through Orbit Determination of Two-Line Element Sets," ESA Space Debris Conference, April 2013.
[6] Oltrogge, D.L. and Alfano, S., "Determination of Orbit Cross-Tag Events and Maneuvers with Orbit Detective," AAS 11-413, Girdwood Alaska, August 2013.
[7] Levit, C. and Marshall, W., "Improved Orbit Predictions Using Two-Line Elements," Elsevier, 11 February 2010.
[8] Oltrogge, D.L. and Kelso, T.S., "Getting to Know Our Space Population From the Public Catalog," AAS 11-416.